Nanotechnology and Nanomaterials

Modeling and Controlling Variations in Advanced 2.5D Packaging Fabrication

C. I. Lang, D. S. Boning
Sponsorship: TSMC

Re-distribution layers (RDLs) are separate packaging layers dedicated to connecting die to one other and to external I/O ports in advanced 2.5D packaging technologies. These layers can be made smaller than the bulky metal traces in conventional substrate packaging, reducing electrical delay and power consumption. Currently, the damascene process is the most common method to create the copper traces in RDLs. However, due to the required inclusion of chemical mechanical polishing (CMP), this process is significantly more expensive than semi-additive electrochemical plating (ECP) and dielectric spin-coating (DSC) processes. The semi-additive techniques are typically avoided as, without CMP, they suffer from thickness variations following the fabrication of each layer. As multiple layers are fabricated, these variations compound and can result in a structure with significant topographical and electrical performance concerns.

Here, we model and predict the non-uniformities in both the DSC (Figure 1) and ECP (Figure 2) process. We first design test vehicles (TVs) which represent topographies common in RDLs, most notably the copper lines and vias, and use these to experimentally determine the thickness variations caused by each process. We then develop empirical models based on these results. The DSC process is modeled as a convolution between the underlying topography (typically the copper lines) and an appropriately chosen impulse response, while the ECP growth rate is modeled as a function of the effective line width and spacings. Finally, we are currently developing and testing dummy fill and cheesing patterns that have the potential to control the variations from both processes. These patterns can be applied to any existing RDL layout, thus ensuring surface planarity without the use of CMP.

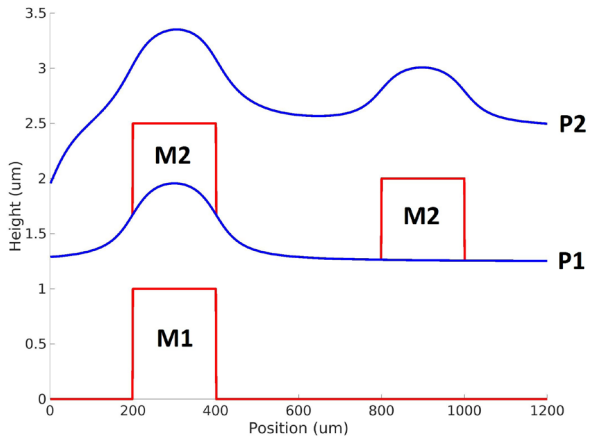

▲Figure 1: Mock RDL cross section consisting of two metal layers and two polyimide layers. Spin coating over non-uniform surfaces leads to variations that carry through to subsequent layers.

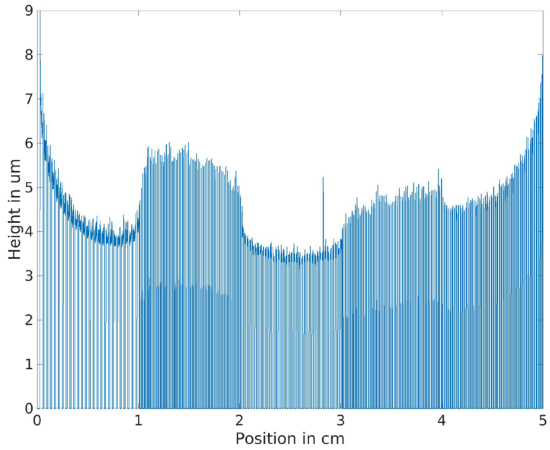

▲Figure 2: Cross section of copper interconnects grown using ECP. Differences in line widths and spacings lead to different growth rates and structural variations.

FURTHER READING

- C. I. Lang and D. S. Boning, "Spin Coating Modeling and Planarization using Fill Patterns for Advanced Packaging Technologies," *Advanced Semiconductor Manufacturing Conference (ASMC)*, [accepted], 2017.
- S. Ho, L. Ding, S. H. Lim, S. A. Sek, M. Yu, and G. Lo, "Polymer-Based Fine Pitch Cu RDL to Enable Cost-Effective Re-Routing for 2.5 D Interposer and 3D-IC," *2013 IEEE 15th Electronics Packaging Technology Conference (EPTC)*, 435-439, 2013.

Online and Incremental Machine Learning Approaches for IC Yield Improvement

H. Chen, D. S. Boning

In the competitive semiconductor manufacturing industry, where large amounts of data are generated, data-driven quality control technologies are gaining increasing importance. In this work, we build machine learning models for high-yield and time-varying semiconductor manufacturing processes. Challenges include class imbalance and concept drift. Class imbalance is due to high manufacturing yield causing small numbers of failure cases compared to passing cases. Concept drift refers to unexpected or unknown changes in the statistical properties of the dataset. Batch and online ensemble machine learning techniques are proposed to address the problem of class imbalance. An incremental learning framework that combines classifiers trained on different data chunks is designed to overcome the problem of concept drift.

We study the packaging and testing process in chip stack flash memory as an application. We build a mathematical model and demonstrate the possibility of yield improvement using a classifier to detect bad dies before packaging. Experimental results demonstrate significant yield improvement potential using real data from industry. Without concept drift, for stacks of 8 dies, an approximately 9% yield improvement can be achieved. In a longer periods of time with realistic concept drift, our incremental learning approach achieves approximately 1.4% yield improvement in the case of a stack of 8 dies and 3.5% in the case of a stack of 16 dies, which are 4.4×× and 1.5×× of the yield improvement using a single classifier trained only on the most recent data.

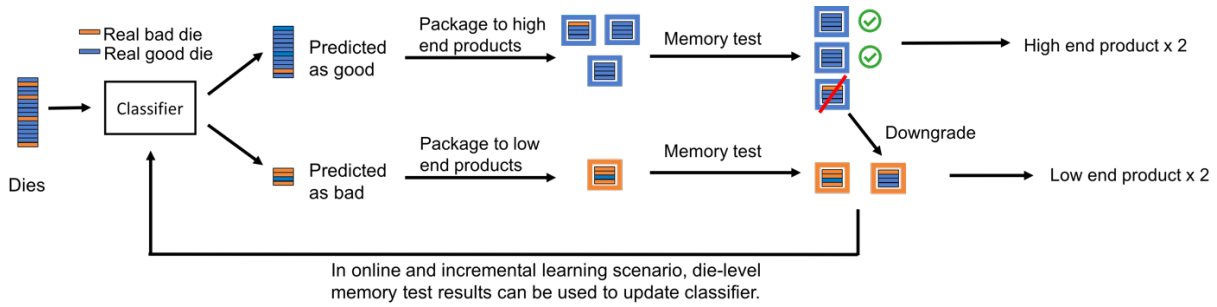

▲ Figure 1: The packaging and memory testing process with a classifier.

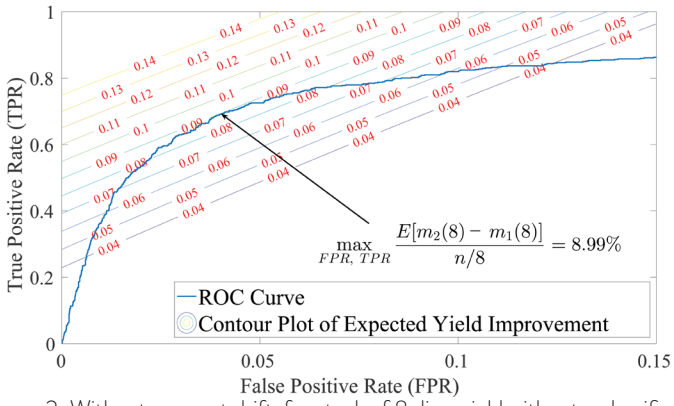

▲ Figure 2: Without concept drift, for stack of 8 dies, yield without a classifier= 77.54%; yield with a classifier= 86.53%, optimal classification threshold=0.68.

FURTHER READING

- H. Chen and D. S. Boning, "Online and Incremental Machine Learning Approaches for IC Yield Improvement," *IEEE/ACM International Conference on Computer Aided Design (ICCAD)*, Irvine, CA, Nov. 2017.

Tensor Recovery for Stochastic Simulation of Nanoscale Devices and Circuits with Many Process Variations

Z. Zhang, T.-W. Weng, L. Daniel
Sponsorship: NSF NEEDS, AIM Photonics

Process variations have become a "red-brick" problem that the semiconductor industry is progressing toward. A random fluctuation at the atomic scale can cause a large impact on the performance of nanoscale and device simulations. In order to increase chip yields, the uncertainties caused by process variations must be well estimated and controlled before a final fabrication. In traditional EDA tools, Monte Carlo-type simulators perform such a task. Recently, stochastic spectral methods have emerged as a promising alternative. They are much more efficient than Monte Carlo simulators for certain design cases, but their efficiency can degrade as the number of process variations increases.

Our approach can efficiently handle design problems with 50 to 60 uncorrelated random parameters. We represent the huge number of device/circuit simulation samples in stochastic collocation by a tensor, which is a representation of a high-dimensional data array. Then, similar to the matrix case, we can exploit the low-rank structure of a tensor to reduce the storage and computational cost, as shown in Figure 1. Combining this low-rank property with the sparse property in high-dimensional generalized polynomial-chaos expansion, we have suggested a low-rank and sparse tensor recovery model. This optimization model allows us to estimate the huge number of unknown simulation samples based on a small number of available simulation results. Therefore, the computational cost can be reduced from an exponential one to a linear one.

This approach has been successfully applied to solve stochastic modeling and simulation problems in microelectromechanical systems (MEMS) design and in complementary metal-oxide semiconductor (CMOS) integrated circuit (IC) design. For the CMOS ring oscillator with 57 uncorrelated process variations in Figure 2, stochastic collocation using a standard deterministic numerical integration requires 1.6E27 simulation samples, whereas our tensor recovery approach only needs 300 simulation samples to construct a highly accurate (with 1% relative error) stochastic model for the oscillator frequency.

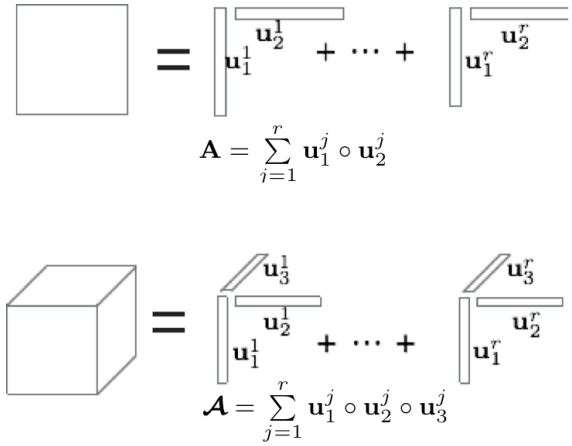

▲ Figure 1: Low-rank decomposition of a matrix (top) and low-rank decomposition of a tensor (bottom). The low-rank decomposition allows representation of high-dimensional data arrays using a few vectors.

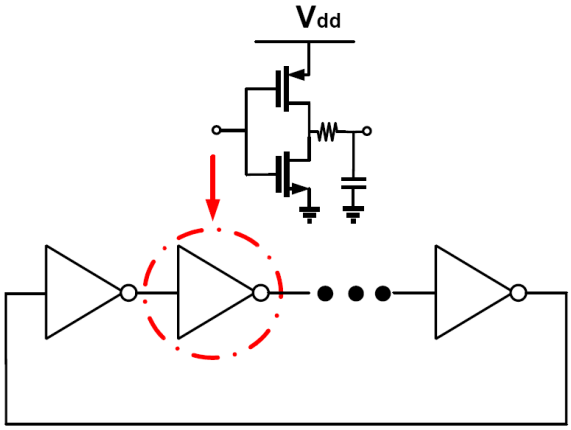

▲ Figure 2: A CMOS ring oscillator. This circuit has 57 independent random parameters describing the variations of transistor threshold voltage, gate oxide thickness, channel length, and width.

FURTHER READING

- Z. Zhang, I. M. Elfadel, and L. Daniel, "Uncertainty Quantification for Integrated Circuits: Stochastic Spectral Methods," *in Proc. Int. Conf. Computer-Aided Design*, 803-810, 2013.
- Z. Zhang, T.-W. Weng, and L. Daniel, "A Big-Data Approach to Handle Process Variations: Uncertainty Quantification by Tensor Recovery," *in Proc. IEEE Workshop on Signal and Power Integrity*, 1-4, 2016.
- Z. Zhang, L. Daniel, K. Batselier, H. Liu, and N. Wong, "Tensor Computation: a New Framework for EDA," *IEEE Trans. CAD of Integrated Circuits and Systems*, [submitted], 2017.

Realizing Monolithic Three-dimensional Integrated Circuits with Emerging Nanotechnologies

T. Srimani, M. Bishop, M. M. Shulaker
Sponsorship: Analog Devices, Inc.

The computing demands of future data-intensive applications far exceed the capabilities of today's electronics and cannot be met by isolated improvements in transistor technologies or integrated circuit (IC) architectures alone. Rather, transformative nanosystems that leverage the unique properties of emerging nanotechnologies to create new three-dimensional IC architectures are required to deliver unprecedented performance and energy efficiency. However, emerging nanomaterials and nanodevices are subject to significant imperfections and variations; thus, realizing functional circuits, let alone transformative nanosystems, has previously been infeasible.

As an example, carbon nanotubes (CNTs) are a promising emerging nanotechnology with exceptional electrical, thermal, and physical properties. Due to these benefits, very-large-scale integrated (VLSI) digital circuits fabricated from carbon nanotube field-effect transistors (CNFETs) are projected to run 3X faster than silicon FinFETs, while simultaneously consuming 3X less energy, resulting in an order-of-magnitude improvement in energy-delay product (EDP, a metric of energy efficiency) for digital VLSI circuits. Despite demonstrations of high performance and scaled CNFETs, realizing VLSI-scale CNFET circuits has previously been prohibited by substantial imperfections and variations to CNTs. For instance, due to the imprecise control over CNT properties, CNTs can be either semiconducting or metallic (metallic CNTs have little or no bandgap and result in increased circuit leakage power and incorrect logic functionality), and non-uniform spacing between CNTs results in variations in the number of CNTs within each CNFET (resulting in degraded noise resilience, increased delay variations, and decreased yield). To overcome these obstacles, we are developing new fabrication and processing techniques, as well as new circuit design techniques. Importantly, while relying on processing or design solutions alone is insufficient, combining approaches allows us to overcome these obstacles and realize, for the first time, energy-efficient VLSI digital systems made from CNFETs.

Additionally, CNFETs present a unique opportunity to radically impact systems beyond providing improved transistors. Specifically, CNFETs enable monolithic 3-D nanosystems, with multiple layers of computation, memory, and sensing densely integrated over the same starting substrate, truly embodying computation immersed in memory and sensing. This is enabled by the very low processing temperatures (<200˚C) of many emerging nanotechnologies (CNFETs for sensors and circuits, and resistive RAM or spin-transfer torque magnetic RAM, for memory). Owing to this monolithic 3-D integration, conventional back-end-of-line inter-layer vias can be used connect vertical layers, which are over 1,000X denser than the through-silicon-vias (TSVs) used with conventional chip-stacking today. We are currently designing, fabricating, and testing monolithic 3-D nanosystem hardware prototypes.

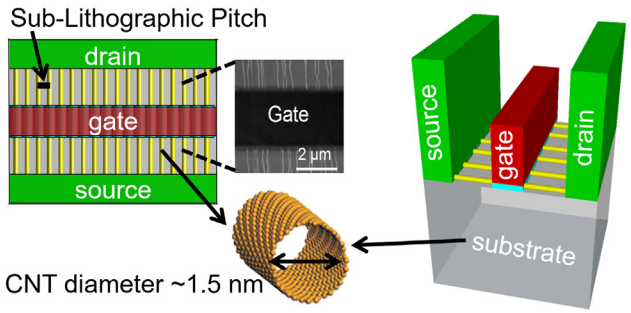

▲ Figure 1: Carbon nanotube field-effect transistor (CNFET).

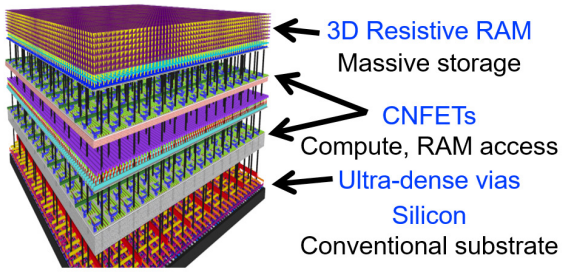

▲ Figure 2: Schematic of a monolithic 3-D IC.

Novel Device Structure for Neuromorphic Computing Array

S. Choi, S. Tan, Y. Kim, J. Kim

Neuromorphic computing has recently emerged as a non-Von Neumann computing method for ultrafast real-time data processing. It utilizes analog switching to represent multiple synaptic weights by varying conductance in the vertical filaments formed in the switching medium, centering around this technology is the memristor which is considered to be a suitable hardware platform for neuromorphic computing. Conventional memristors typically utilize a defective amorphous solid as a switching medium for defect-mediated formation of conducting filaments. However, the imperfection of the switching medium also causes stochastic filament formation, leading to spatial and temporal variation of the devices. Our group proposes a silicon-based epitaxial random access memory (epiRAM), where we precisely confine the conducting paths in the single-crystalline films, resulting in unprecedented device performances. MIT's epiRAM exhibits extremely low temporal/spatial variation, linear synaptic weight update, high on/off ratio, great endurance, long retention time, and self-selectivity. This performance is suitable for large-scale neuromorphic computing hardware. Figure 1 shows cycle-to-cycle set voltage variation for 700 switching cycles, and Figure 2 shows analog behavior of the epiRAM where we obtain linear potentiation and depression.

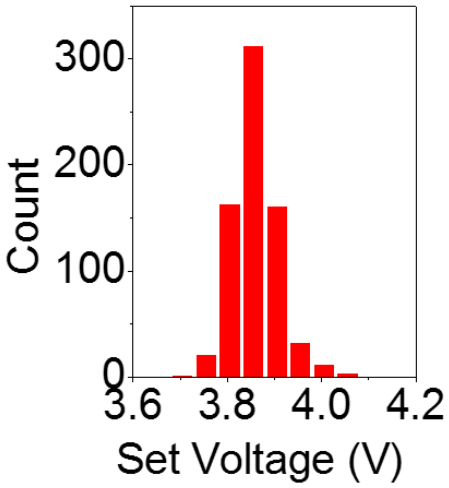

▲ Figure 1: Cycle-to-cycle variation.

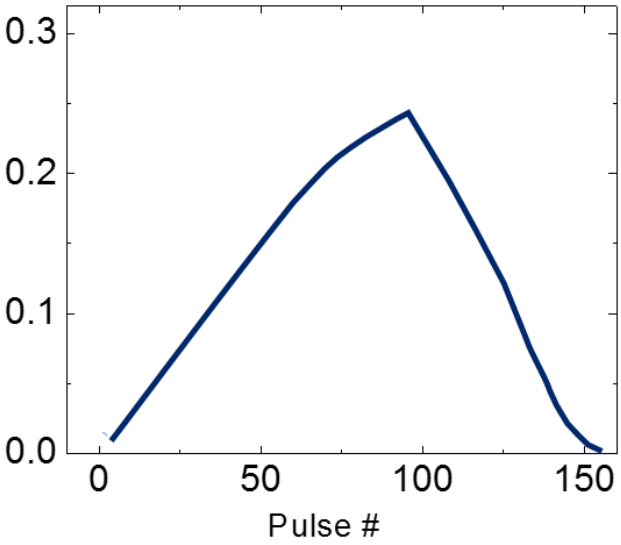

▲ Figure 2: Linear potentiation and depression.

FURTHER READING

- S. Choi, S. Tan, Y. Kim, C. Heidelberger, P. Chen, S. Yu, and J. Kim, "Uniform Epitaxial Memory Towards Large-Scale Neuromorphic Arrays," *Nature*, under review, 2017.

Remote Epitaxy through Graphene for Two-Dimensional Material Based Layer Transfer

Y. Kim, S. Cruz, K. Lee, K. Qiao, J. Kim
Sponsorship: Masdar Institute of Science and Technology, LG Electronics

Van der Waals epitaxy (vdWE) has gained great interest for crystalline growth as it substantially relaxes the strict lattice matching requirements in conventional heteroepitaxy and allows for facile layer release from the vdW surface. In recent studies, vdWE was investigated on two-dimensional (2D) materials grown or transferred on arbitrary substrates, with the primary notion that the 2D material is the sole epitaxial seed layer in vdWE. However, the underlying substrate may still play a role in determining the orientation of the overlayers since the weak vdW potential field from 2D materials may barely screen the stronger potential field from the substrates.

Here, we reveal that the epitaxial registry of adatoms during epitaxy can be assigned by the underlying substrate remotely through 2D materials by modulating the interaction gap between the substrate and the epilayer. Our study shows that remote epitaxial growth can be performed through a single-atom-thick gap defined by monolayer graphene at the substrate-epilayer interface. Simulations using density functional theory (DFT) prove that remote epitaxy can occur within a ~9 Å substrate-epilayer gap. We experimentally demonstrate successful remote homoepitaxy of GaAs(001) on GaAs(001) substrates through monolayer graphene (Figure 1). The concept is extended for remote epitaxy of other semiconductors such as InP and GaP. The grown single-crystalline films are then rapidly released from the vdW surface of graphene. To prove the functionality of GaAs film grown via remote homoepitaxy, we have successfully grown and fabricated light emitting diodes (LEDs) on graphene/GaAs substrate (Figure 2). This concept, here termed 2D material based layer transfer (2DLT), suggests a method to copy/paste any type of semiconductors films from the underlying substrates through 2D materials then rapidly released and transferred to the substrates of interest. With the potential to reuse graphene-coated substrates, 2DLT will greatly advance non-Si electronics and photonics by displacing the high cost of non-Si substrates.

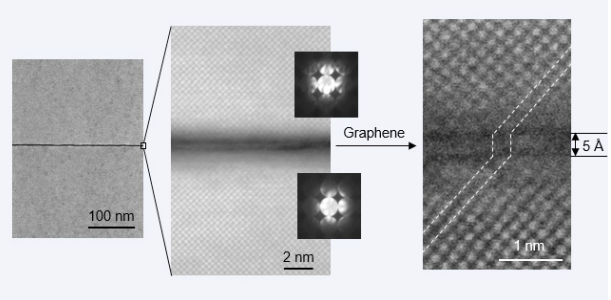

▲Figure 1: High resolution STEM images showing excellent remote alignment of the (001) GaAs lattices through the graphene. Convergent beam electron diffraction patterns (001) from the epilayer (top) and the substrate (bottom) show identical zinc blend (001) orientations.

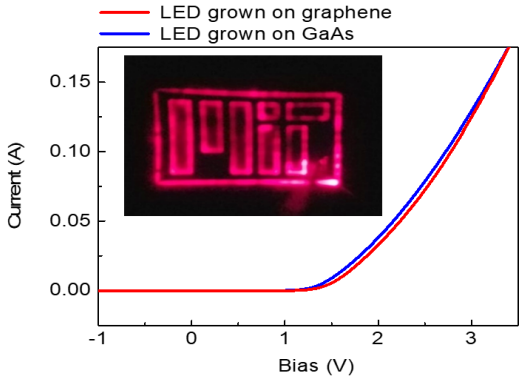

▲Figure 2: *I-V* curves of LEDs grown on graphene/GaAs substrates and directly on GaAs. Inset exhibits the emitted red light from the LEDs grown on the graphene/GaAs substrate.

FURTHER READING

- Y. Kim, S. Cruz, K. Lee, B. O. Alawode, C. Choi, Y. Song, J. M. Johnson, J. Kim, et al., "Remote Epitaxy through Graphene for Two-Dimensional Material Based Layer Transfer," *Nature*, 544(7650), 340-343, 2017.

Epitaxy: Programmable Atom Equivalents versus Atoms

M. X. Wang, S. E. Seo, P. A. Gabrys, D. Fleischman, B. Lee, Y. Kim, H. A. Atwater, R. J. Macfarlane, C. A. Mirkin
Sponsorship: AFOSR, NSF

The programmability of DNA makes it an attractive structure-directing ligand for the assembly of nanoparticle (NP) superlattices in a manner that mimics many aspects of atomic crystallization. These superlattices have potential application as sensors, waveguides, or structural materials due to their unique optical, mechanical, and other physical properties. However, integrating these materials into devices requires complete control over lattice structure and shape, and the synthesis of multilayer single crystals of defined size remains a challenge. Though previous studies considered lattice mismatch as the major limiting factor for multilayer assembly, thin film growth depends on many interlinked variables. In preliminary work in the Macfarlane Laboratory, a more comprehensive approach has been taken to study fundamental elements of assembly, such as the growth temperature and the thermodynamics of interfacial energetics, to achieve epitaxial growth of NP thin films. Under equilibrium conditions, single crystalline, multilayer thin films can be synthesized over 500 × 500 μm² areas on lithographically patterned templates (Figure 1), whereas deposition under kinetic conditions leads to the rapid growth of glassy films. Importantly, these superlattices follow the same patterns of crystal growth demonstrated in atomic thin film deposition, allowing these processes to be understood in the context of well-studied atomic epitaxy and enabling a nanoscale model to study fundamental crystallization processes. Through understanding the role of epitaxy as a driving force for NP assembly, we are able to realize 3-D architectures of arbitrary domain geometry and size.

Single-crystal alignment is achieved through the introduction of an epitaxial driving force. Gold posts are patterned on a silicon substrate using conventional electron beam lithography (EBL) techniques and electron beam evaporation. The posts are commensurate in size and shape to the gold NPs utilized and functionalized with DNA. When the posts are positioned to mimic a continuous (100) plane of a body-centered cubic (bcc) superlattice with arbitrary macroscopic shape (Figure 2), the DNA-NPs self-assemble atop the pattern, maintaining epitaxy.

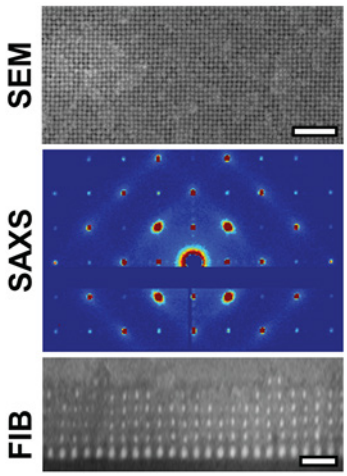

▲ Figure 1: Scanning electron microscopy (SEM), small-angle X-ray scattering, and SEM of cross-section following focused-ion beam (FIB) milling of a 10-layer DNA-NP epitaxial thin film. Scale bars for SEM and FIB are 500 and 200 nm, respectively.

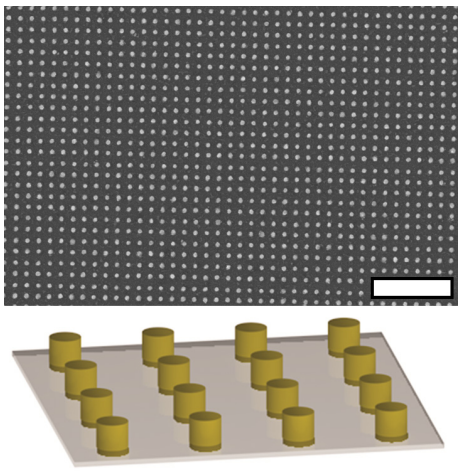

▲ Figure 2: Schematic of substrate patterned by EBL. Gold posts are designed to mimic the size, shape, and placement of the DNA-NP gold cores in the (100) plane of a bcc arrangement.

FURTHER READING

- S. L. Hellstrom, Y. Kim, J. S. Fakonas, A. J. Senesi, R. J. Macfarlane, C. A. Mirkin, and H. A. Atwater, "Epitaxial Growth of DNA-Assembled Nanoparticle Superlattices on Patterned Substrates," *Nano Lett.*, vol. 13, no. 12, 6084-6090, Nov. 2013.
- S. Pan, T. I. N. G. Li, and M. Olvera de la Cruz, "Molecular Dynamics Simulation of DNA-Directed Assembly of Nanoparticle Superlattices using Patterned Templates," *J. Polymer Science B*, vol. 54, no. 17, 1687-1692, May 2016.
- M. X. Wang, S. E. Seo, P. A. Gabrys, D. Fleischman, B. Lee, Y. Kim, H. A. Atwater, R. J. Macfarlane, and C. A. Mirkin, "Epitaxy: Programmable Atom Equivalents Versus Atoms," *ACS Nano*, vol. 11, no. 1, 180185, Dec. 2016.

Sub-10-nm Patterning via Self-Assembled Block Copolymer and Vapor-Phase Deposited Topcoat

D. H. Kim, H. S. Suh, P. Moni, S. Xiong, L. E. Ocola, N. J. Zaluzec, K. K. Gleason, P. F. Nealey
Sponsorship: NSF

The semiconductor industry has made a great effort to produce sub-10-nm patterns in a cost-effective way as the feature size is getting close to the limit of the wavelength of the UV light source in current photolithography. As an enabling technology, block copolymers (BCP) can be self-assembled to nanoscale structures by thermal anneal with no UV light. In particular, for sub-10 nm patterning, we developed a new technology employing directed self-assembly (DSA) of highly segregating BCP and a topcoat deposited by initiated chemical vapor deposition (iCVD). iCVD, a dry process, enabled the deposition of a crosslinked polymeric topcoat on the BCP films without any damage to the BCP films. We here discovered that the iCVD made a unique interface between the BCP films and topcoat through grafting intrinsically. The interface achieves a non-preferential surface for domains of the multiple BCPs, thereby resulting in the desirable perpendicular orientation of the BCP domains. In addition, because the crosslinked topcoat is chemically durable against solvents of e-beam resist, we could fabricate additional topcoat patterns on the BCP films by e-beam lithography. The post-patterning enabled by iCVD permits positioning of a sub-10-nm patterning area on a Si wafer, which is more beneficial to the interconnect devices in the semiconductor industry.

Figure 1 shows sub-10-nm line-and-space patterns behind a micron size letter pattern, "a," after DSA and dry etching. Figure 1 confirms that the patterned iCVD topcoat (red) beneath the e-beam resist pattern is holding a sub-10-nm domain, achieving dual-scale patterns. Then, we successfully transferred the patterns to a Si wafer by a dry etching process as seen in Figure 2. As the iCVD process can be readily scaled up to a larger area, we anticipate that iCVD topcoats will enable the widespread implementation of DSA in nanomanufacturing to create sub-10-nm scale patterns.

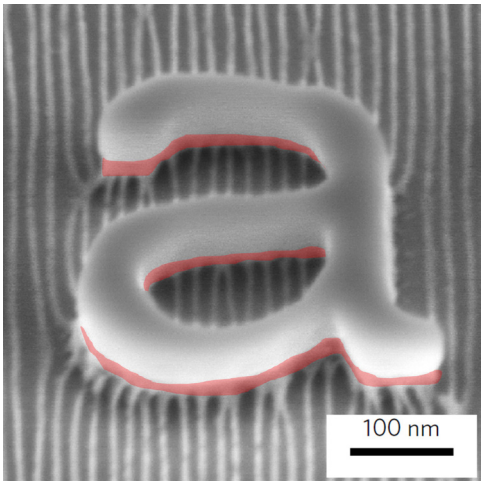

▲ Figure 1: Scanning electron microscopic (SEM) images of dual-scale alumina patterns with vapor phased topcoat (red) beneath e-beam resist. The topcoat assists the perpendicular orientation of BCP domains, thereby creating sub-10-nm line-and-space patterns behind a micro-size letter pattern.

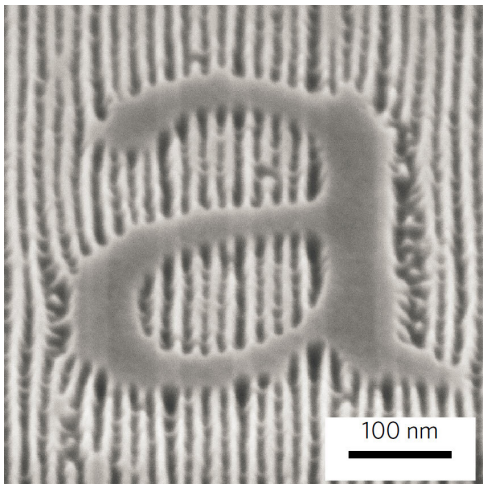

▲ Figure 2: SEM images of Si patterns after transferring with the mask in Figure 1.

FURTHER READING

- H. S. Suh, D. H. Kim, P. Moni, S. Xiong, L. E. Ocola, N. J. Zaluzec, K. K. Gleason, and P. F. Nealey, "Sub-10 nm Patterning via Directed Self-Assembly of Block Copolymer Films with a Vapour-Phase Deposited Topcoat," *Nature Nanotechnology*, 12, 575, 2017.

Experimental Characterization and Modeling of Templated Solid-State Dewetting of Thin Single-Crystal Ni Films

Y. A. Shin, G. H. Kim, S. Jahangir, R. V. Zucker, J. Ye, W. Ma, B. Yildiz, W. C. Carter, C. V. Thompson
Sponsorship: NSF

Templated solid-state dewetting provides a simple method for film patterning to form complex structures (Figure 1). The patterns that result from solid state dewetting are affected by various instabilities that develop at retracting edges and the features they lead to. These include pinch-off to form wires parallel to retracting film edges, instabilities at corners in retracting edges ("corner instabilities"), and Rayleigh-like instabilities that lead to break up of wire-like features. Previously we reported on the strong effects of crystalline anisotropy on the Rayleigh-like instability and identified factors that stabilize wire-like features. In the past year, we reported on experimental characterization and modeling of the corner instability and established the conditions that lead to the development of the unstable edge retraction when corners are present in film edges. We also characterized the effects of the annealing ambient on anisotropy in the rate of edge retraction and consequent changes in the patterns that form as a result of dewetting. We found that changing the gases and gas flow rates during annealing causes surface reconstructions that affect the anisotropy of the energy of the surfaces of the films and the anisotropy of surface diffusion. Control of the ambient gas during annealing provides an additional means of controlling the types of patterns that result from simple templating.

We are currently focusing on a fingering instability that can occur during edge retraction and results in formation of parallel wire-like features with different orientations from those that develop as a result of rim-pinch-off (Figure 2). Understanding and controlling whether pinch-off or fingering occurs is important for development of techniques for controlled pattern formation. When fingering occurs, it is also desirable to control the size and spacing of wires that form. In the past year, we have demonstrated that the initial roughness of a film edge determines whether pinch-off or fingering occurs, with rough edges leading to fingering. To further understand this phenomenon and to control it, we have used edges with controlled patterned roughness to template the fingering instability. We have found that the spacing of wires formed due to fingering can be controlled by the period of the patterned roughness. We have also found that controlling the period of the fingering process affects the kinetics of the fingering. Our ability to control the fingering process allows us to develop kinetic models that can be used to design templates that will lead to specific complex structures during solid-state dewetting. Through these studies, we are developing a suite of methods that can be used to suppress dewetting when it is undesirable and to control it for use in pattern formation.

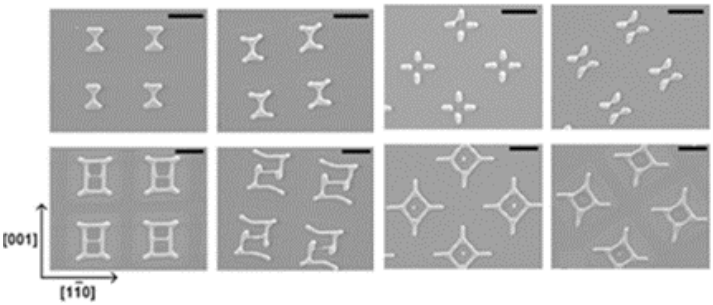

▲ Figure 1: Patterns formed by solid state dewetting of square patches of Ni films patterned with different sizes and crystallographic orientations.

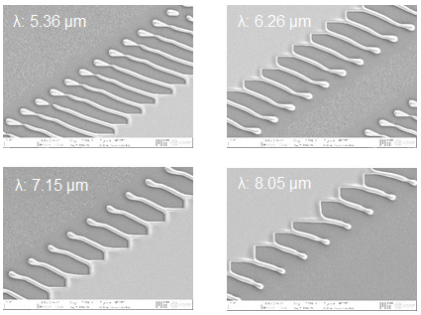

▲ Figure 2: Wires formed by templating a fingering instability using patterned periodic edge roughness.

FURTHER READING

- C. V. Thompson, "Solid-state Dewetting of Thin Films," Annual Review of Materials Research, vol. 42, 399-434, 2012.
- R. V. Zucker, G. H. Kim, J. Ye, W. C. Carter, and C. V. Thompson, "The Mechanism of Corner Instabilities in Single-Crystal Thin Films During Dewetting," J. Appl. Phys., vol. 119, 125306, 2016.
- G. H. Kim, W. Ma, B. Yildiz, and C. V. Thompson, "Effect of Annealing Ambient on Anisotropic Retraction of Film Edges During Solid-State Dewetting of Thin Single Crystal Films," J. Appl. Phys. vol. 120, 075306, 2016.

Coherent Soft X-Ray Diffractive Imaging of Magnetic Nanotextures

J. Li, J. Pelliciari, R. Comin
Sponsorship: MIT Startup Funds

The ability to image the nanoscale structure of materials with tunable magnetic textures is pivotal for the development of low-power and nonvolatile data storage technologies. Soft X-ray imaging has emerged in the last decade as a powerful and accurate methodology to resolve the bulk domain structure of several magnetic materials—magnetic multilayers, buried interfaces, or skyrmion lattices—as well as nanoelectronic devices under operating conditions.

Soft X-ray imaging relies on two main requirements: (i) the ability to focus a collimated X-ray beam on a spot the size of a few tens of nm and (ii) the development of algorithms capable of inverting the information in reciprocal space (diffraction pattern) back to real space. We have recently commissioned a new soft X-ray nanofocusing setup installed at beamline CSX-1 of the National Synchrotron Light Source II. The schematics of this setup are shown in Figure 1. A key element is the Fresnel zone plate (Figure 1a), fabricated at MTL, which acts as a diffractive phase mask to focus X-rays to a 70-nm spot at the sample. The beam spot can be moved with the aid of piezo-based nanopositioners (Figure 1b), which translate the X-ray optics while keeping the sample in a fixed position. Diffracted X-rays are collected with a CCD camera in the far field (~30 cm from the sample). The resulting speckle pattern (Figure 1c) encodes the information on the nanoscale magnetic texture in reciprocal (Fourier) space and can be acquired in less than a second. By Fourier-inverting back onto real space, we can unveil the domain structure in real space with an ultimate accuracy of 10-20 nm (Figure 1d).

We plan to apply this new method to the study of magnetic materials in their pure state (single crystal or thin films) as well as in a device configuration, where the use of a contactless probe enables the study of the material or device response *in operando*. Our future focus is on transition metal- and rare-earth-based compounds, particularly those exhibiting antiferromagnetic order, which can be switched on very fast (picosecond) timescales.

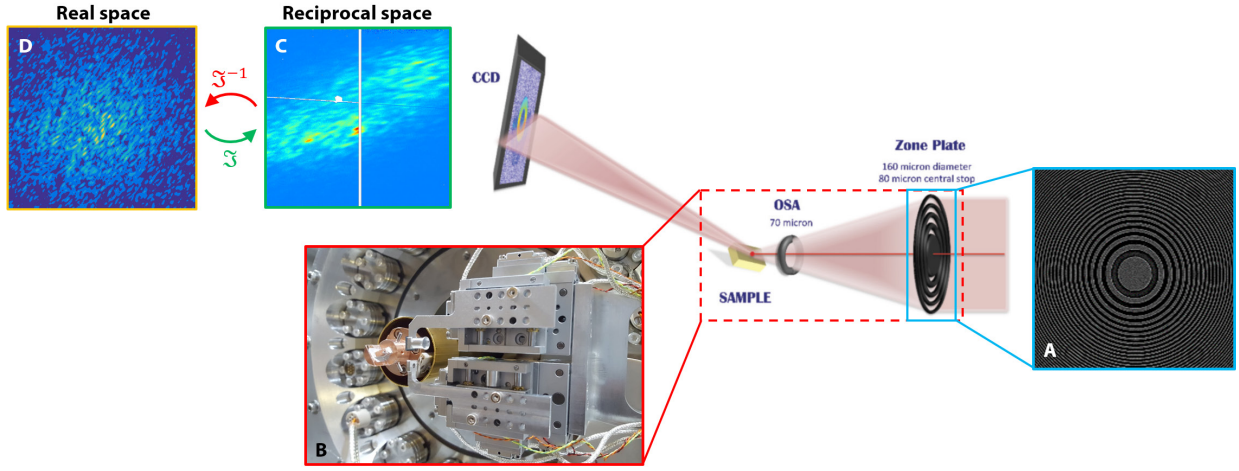

▲ Figure 1: Coherent soft X-ray diffraction setup at the National Synchrotron Light Source II. Main panel: schematics of the X-ray optics used in coherent diffraction; a Fresnel zone plate (fabricated at MTL; SEM image in (a) focuses X-rays down to a ~70- nm spot at the sample position; diffracted X-rays are imaged with a CCD camera, (b) inside view of the diffraction chamber, with piezo-actuated nanopositioners located upstream of the sample stage (copper), (c & d) example of speckle pattern (c) from antiferromagnetic domain structure of a $NdNiO_3$ thin film, and corresponding reconstructed domain pattern in real space (d). C and d are related by a Fourier transform.

FURTHER READING

- A. Tripathi, J. Mohanty, S. H. Dietze, O. G. Shpyrko, E. Shiptona, E. E. Fullerton, S. S. Kim, and I. McNulty, "Dichroic Coherent Diffractive Imaging," in *Proc. National Academy of Sciences*, vol. 108, 13393-13398, 2011.
- S. Roy, D. Parks, K. A. Seu, R. Su, J. J. Turner, W. Chao, E. H. Anderson, S. Cabrini, and S. D. Kevan, "Lensless X-Ray Imaging in Reflection Geometry," *Nature Photonics*, vol. 5, 243-245, 2011.
- J. Miao, T. Ishikawa, I. K. Robinson, M. M. Murnane, "Beyond Crystallography: Diffractive Imaging using Coherent X-Ray Light Sources," *Science*, vol. 348, 530-535, 2015.

Information Limit of Domain-Wall-Based Nanowire Devices

S. A. Siddiqui, S. Dutta, C. A. Ross, M. A. Baldo
Sponsorship: NSF

Spintronic and magnetic devices use the spin of electrons instead of their charge to implement ultra-low-power logic and memory applications. In domain-wall-based magnetic devices, charge or spin currents move the boundary between different magnetic domains in a nanowire. Rather than flipping the orientation of the entire wire at once, this incremental approach improves the energy efficiency. Domain walls, however, can be pinned by the line edge roughness of nanowires, affecting the operation of the devices. Notches created by edge roughness comparable to the width of domain walls have been identified as the most effective pinning sites for domain walls, although the precise relation between the line edge roughness and domain wall pinning sites is unknown. Here, we show the autocorrelation of pinning sites with the line edge roughness in sub-100-nm-wide Co-wires. We have shown both experimentally and with simulation that the correlation length of edge roughness defines the effective pinning site distribution for domain walls in individual nanowires. If we apply a self-affine model for the intrinsic roughness of fabricated edges, our result identifies the limit for information density in magnetic nanowires used in both domain-wall-based logic and memory devices.

FURTHER READING

- J. A. Currivan-Incorvia, S. A. Siddiqui, S. Dutta, E. R. Evarts, J. Zhang, D. Bono, C. A. Ross, and M. A. Baldo, "Logic Circuit Prototypes for Three-Terminal Magnetic Tunnel Junctions with Mobile Domain Walls," *Nature Comm.*, vol. 7, 10275, 2016.
- S. S. P. Parkin, M. Hayashi, and L. Thomas, "Magnetic Domain-Wall Racetrack Memory," *Science*, vol. 320, 190–194, 2008.

Layer-Dependent Ferromagnetism in a van der Waals Crystal Down to the Monolayer Limit

D. R. Klein, E. Navarro-Moratalla, B. Huang, G. Clark, R. Cheng, K. Seyler, D. Zong, E. Schmidgall, M. A. McGuire, D. H. Cobden, W. Yao, D. Xiao, P. Jarillo-Herrero, X. Xu
Sponsorship: NSF, U. S. Department of Energy, Gordon and Betty Moore Foundation

Since the discovery of graphene just over a decade ago, the field of 2D materials has expanded to include a broad range of materials including conductors, insulators, semiconductors, and superconductors. Surprisingly, no intrinsic magnets made it into the 2D materials family until just very recently. In a study published in *Nature*, our group along with collaborators at the University of Washington have, for the first time, experimentally demonstrated long-range ferromagnetic order in an atomically-thin crystal, chromium triiodide (CrI_3), down to the monolayer limit (crystal structure shown in Figure 1). This is the first ferromagnet in the family of 2D materials. In the same way, in which graphene permitted studying the transport of electrons in a true 2D lattice, monolayer CrI_3 opens the door for the study of magnetism in the true 2D limit.

We first cleave bulk crystals of CrI_3 down to few-layer flakes, including monolayer flakes just one unit cell (three atoms) thick. Then, we probe the materials using magneto-optical Kerr effect (MOKE) spectroscopy, which reveals the out-of-plane magnetization of the field. We reveal a dramatic dependence of the magnetic ground states on the number of layers in a CrI_3 crystal. First, we observe 2D Ising ferromagnetic behavior of the monolayer below its Curie temperature of 45 K (Figure 2). Moreover, bilayer CrI_3 crystals exhibit antiferromagnetism, which can be explained by the two layers of the crystal containing opposite spins that cancel each other out to reveal a net zero magnetization. By just adding one additional layer to bilayer CrI_3, one recovers a strong out-of-plane magnetization in the trilayer crystal as the interlayer coupling constant switches sign. Our results pave the way for further studies of interfacing 2D CrI_3 with other atomically-thin materials in van der Waals heterostructures, which could revolutionize technologies in magnetoelectronics, information, and spin-based data storage.

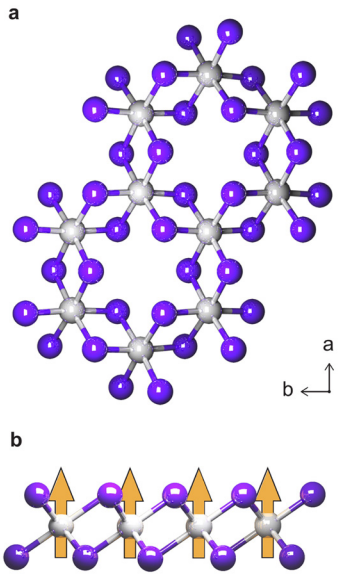

▲ Figure 1: Crystal structure of CrI_3 as viewed along the (a) **c**-axis (top-down) and (b) **a**-axis (in-plane). Cr^{3+} and I^- ions are displayed in white and purple, respectively.

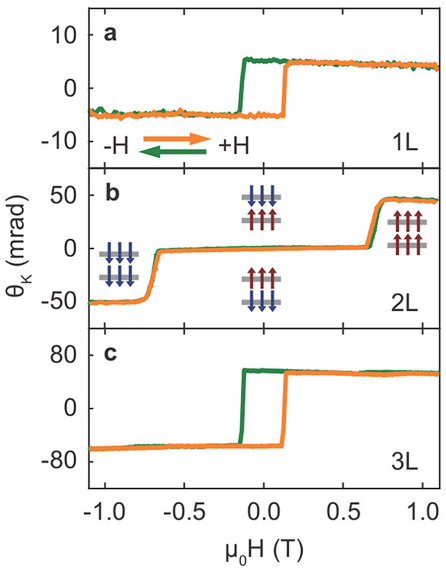

▲ Figure 2: Polar MOKE signals of (a) monolayer, (b) bilayer, and (c) trilayer flakes of CrI_3 as a function of applied magnetic field.

FURTHER READING

- B. Huang, G. Clark, E. Navarro-Moratalla, D. R. Klein, R. Cheng, K. Seyler, D. Zhong, E. Schmidgall, M. McGuire, D. Cobden, W. Yao, D. Xiao, P. Jarillo-Herrero, and X. Xu, "Layer-Dependent Ferromagnetism in a van der Waals Crystal Down to the Monolayer Limit," *Nature* 546, 270-273, 2017.

Room Temperature Spin-Orbit Torque Switching Induced by a Topological Insulator

J. Han, S.A. Siddiqui, J. Finley, L. Liu, A. Richardella, N. Samarth
Sponsorship: NSF

Recent studies on the topological insulators (TI) have attracted great attention due to the rich spin-orbit physics and promising applications in spintronic devices. In particular, the strongly spin-moment coupled electronic states have been extensively pursued to realize efficient spin-orbit torque (SOT) switching. However, so far current-induced magnetic switching with TI has been observed only at cryogenic temperatures. Whether the topologically protected electronic states in TI could benefit from spintronic applications at room temperature remains a controversial issue.

In this work, we report SOT switching in a TI/ferromagnet heterostructure with perpendicular magnetic anisotropy (PMA) at room temperature. Ferrimagnetic cobalt-terbium (CoTb) alloy with robust bulk PMA is directly grown on a classical TI material, Bi_2Se_3. The low switching current density provides definitive proof of the high SOT efficiency from TI and suggests the topological spin-momentum locking in TI even if it is neighbored by a strong ferromagnet. Furthermore, the effective spin Hall angle of TI is determined to be several times larger than commonly used heavy metals. Our results demonstrate the robustness of TI as an SOT switching material and provide an avenue towards applicable TI-based spintronic devices.

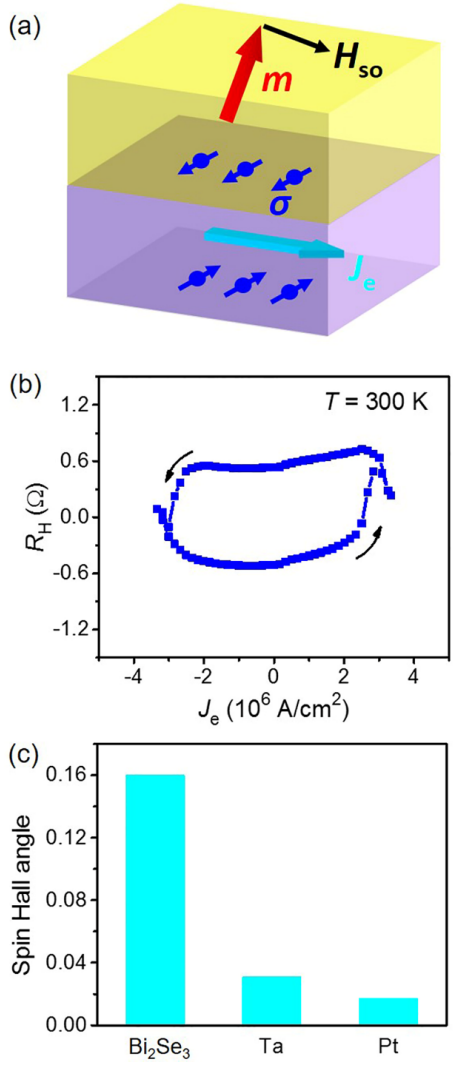

▲ Figure 1: (a) Schematic of SOT in Bi2Se3/CoTb heterostructure. (b) Room temperature SOT switching in Bi2Se3/CoTb. Hall resistance is measured when sweeping a direct current (DC) under a bias magnetic field along the current direction. (c) Absolute values of the effective spin Hall angles of Bi2Se3, Pt, and Ta measured by our experiments.

Spin-Orbit Torque in Compensated Ferrimagnetic Cobalt-Terbium Alloys

J. Finley, L. Liu
Sponsorship: NSF, SRC

Spintronic devices promise to be an energy-efficient alternative to complementary metal-oxide semiconductor devices for logic and memory. However, in order to be more competitive, further reductions in switching energy and switching speed are needed. There has been great interest recently in using antiferromagnetically coupled materials as opposed to ferromagnetic materials to store information. Compared with ferromagnetic materials, antiferromagnetically coupled systems exhibit fast dynamics as well as immunities against perturbations from external magnetic fields, potentially enabling spintronic devices with higher speed and density. Despite the potential advantages of information storage in antiferromagnetically coupled materials, it remains unclear whether one can control the magnetic moment orientation efficiently because of the canceled magnetic moment.

Here, we report spin-orbit torque induced magnetization switching of ferromagnetic $Co_{1-x}Tb_x$ thin films (Figure 1). By varying the relative concentrations of the two atomic species, one can reach compensation points where the net magnetic moment or angular momentum goes to zero. We demonstrate current induced switching in all of the studied film compositions, including those near the magnetization compensation point. We then quantify the spin-orbit torque induced effective magnetic field, where we find that close to the compensation point, there is a divergent behavior that scales with the inverse of magnetization (Figure 2), which is consistent with the conservation of angular momentum. Moreover, we also quantified the Dzyaloshinskii-Moriya interaction (DMI) energy in the $Ta/Co_{1-x}Tb_x$ system, and we found that the energy density increases as a function of the Tb concentration. This tunable DMI could be potentially useful for spintronic applications that employ stable magnetic textures for information storage. The large effective spin-orbit torque, the previously demonstrated fast dynamics, and the minimal net magnetization in these ferrimagnetic systems promise spintronic devices that are faster and more scalable than traditional ferromagnetic systems.

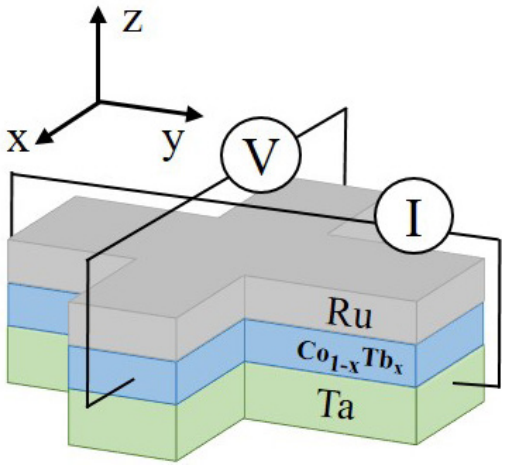

▲ Figure 1: Schematic of the film stack and Hall bar device geometry. A ferrimagnetic $Co_{1-x}Tb_x$ layer is sandwiched between the Ta spin-torque generating layer and a Ru capping layer.

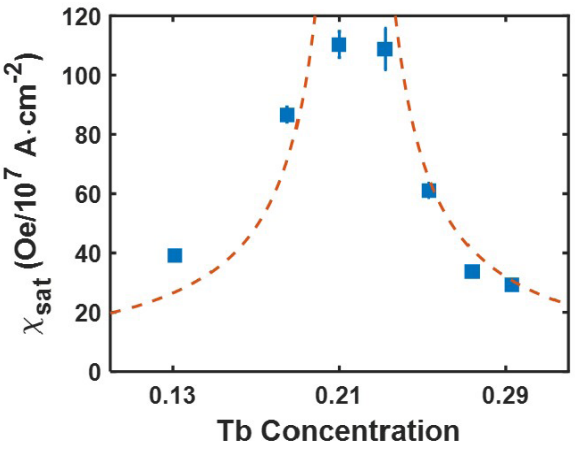

▲ Figure 2: Saturation efficiency χ_{sat}, which is proportional to the spin-orbit torque effective magnetic field, for different $Co_{1-x}Tb_x$ films. The saturation efficiency is largest near the magnetic moment compensation point.

FURTHER READING

- J. Finley and L. Liu, "Spin-Orbit-Torque Efficiency in Compensated Ferrimagnetic Cobalt-Terbium Alloys," *Phys. Rev. Applied*, vol. 6, 054001, Nov. 2016.
- T. Jungwirth, X. Marti, P. Wadley, and J. Wunderlich, "Antiferromagnetic Spintronics," *Nat. Nanotechnol.*, vol. 11, no. 3, 231–241, Mar. 2016.
- L. Liu, C.-F. Pai, Y. Li, H. W. Tseng, D. C. Ralph, and R. A. Buhrman, "Spin-Torque Switching with the Giant Spin Hall Effect of Tantalum," *Science*, vol. 336, no. 6081, 555–558, May 2012.

Research on CMOS-Compatible High-K Dielectrics for Magneto-Ionic Memory

S. Kim, H. L. Tuller, in collaboration with A. J. Tan, G. S. Beach
Sponsorship: CMSE, Interdisciplinary Research Groups, NSF

High-k dielectrics play a key role in modern microelectronic circuitry, given their ability to provide reduced leakage currents while providing adequate capacitance in ever smaller nano-dimensioned metal-oxide semiconductor field-effect transistor (MOSFET) devices. Recently, the Beach group at MIT demonstrated the ability to modulate the magnetic properties of transition metal thin-films by electrical bias across thin-films of Gd_2O_3 (Figure 1). The reversible switching was demonstrated to be assisted by the electro-migration of oxygen ions to and away from the transition metal/Gd_2O_3 interface. This novel process, now called "magneto-ionic control," creates new opportunities for nonvolatile information storage.

Previous research showed that the device's operation depends on the thickness of the dielectric layer, its interaction with the ambient atmosphere, and the device's temperature. These dependencies suggest that this magneto-ionic device is an electrochemical device operating via interfacial reaction, migration, and diffusion. However, questions remain about the origins of its mechanisms. In this study, we intend to establish a strategy for enhancing the performance of the device by investigating the underlying operating mechanisms; we ultimately hope to test the potential of this novel device in memory applications. To understand the diffusion in the oxide layer, we have undertaken a detailed examination of the properties of Gd_2O_3, a model oxide, and related oxides as well as investigated device design to implement studies with controlled parameters.

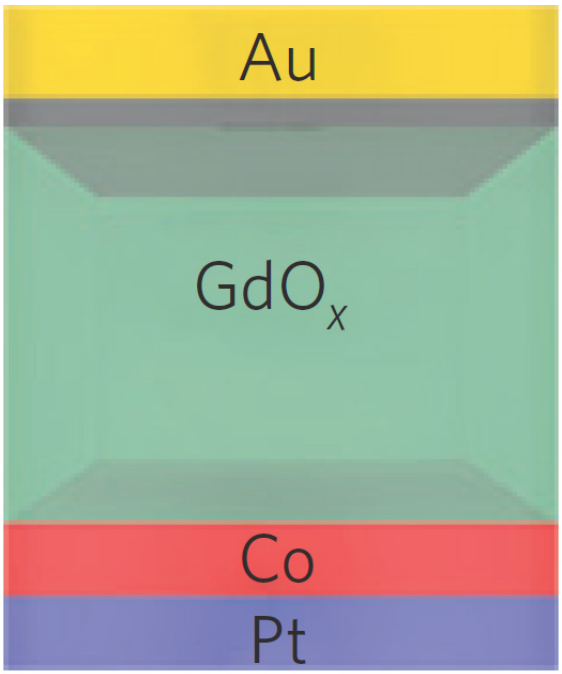

▲ Figure 1: Structure of magneto-ionic device.

FURTHER READING

- U. Bauer, L. Yao, A. J. Tan, P. Agarwal, S. Emori, H. L. Tuller, S. van Dijken, and G. Beach, "Magneto-Ionic Control of Interfacial Magnetism," *Nature Materials*, vol. 14, 174-181, 2015.

CVD Growth of High-Quality Transition Metal Dichalcogenide Monolayers and their Intrinsic Electronic Transport Properties

P.-C. Shen, J. Kong
Sponsorship: NSF E3S

Monolayer transition metal dichalcogenides (TMDs) such as molybdenum disulfide (MoS_2) and tungsten disulfide (WS_2) have been attractive for use in ultra-scaled electronic and optoelectronic devices because of their atomically thin thicknesses, direct band gaps, and strong spin-orbit interactions. Technologies for the mass-production of high-quality, large-area, and atomically thin TMD films or single-crystal grains are highly needed in order to bring them to practical applications. Our group has developed reliable methods for growing high-quality monolayer MoS_2 and WS_2 via chemical vapor deposition (CVD) and investigated their intrinsic and high-k dielectrics enhanced electrical transport properties for device applications. Our group has also focused on defect characterization of TMDs.

Figure 1 shows the photo and optical images of the as-grown monolayer MoS_2 films and single-crystal domains. The continuous area of the MoS_2 thin films grown in this work is typically ~1 cm x 1cm. The triangular domain of MoS_2 single crystals can be found at the edges of the continuous region with a side length as large as ~ 60 μm. Our CVD-grown MoS_2 films show a PL to Raman peak intensity ratio as high as ~ 100 and a full-width-half-maximum as small as ~ 55 meV, suggesting an excellent optical quality. The peak room-temperature field-effect mobility of MoS_2 reaches ~ 18 $cm^2 V^{-1} S^{-1}$. On the other hand, Figure 2 presents the optical images and electrical transport properties of the CVD-grown WS_2 monolayers. The as-grown WS_2 exhibits n-type semiconducting behavior with a direct band gap at 1.97 eV and a field-effect mobility of ~ 7 $cm^2 V^{-1} S^{-1}$.

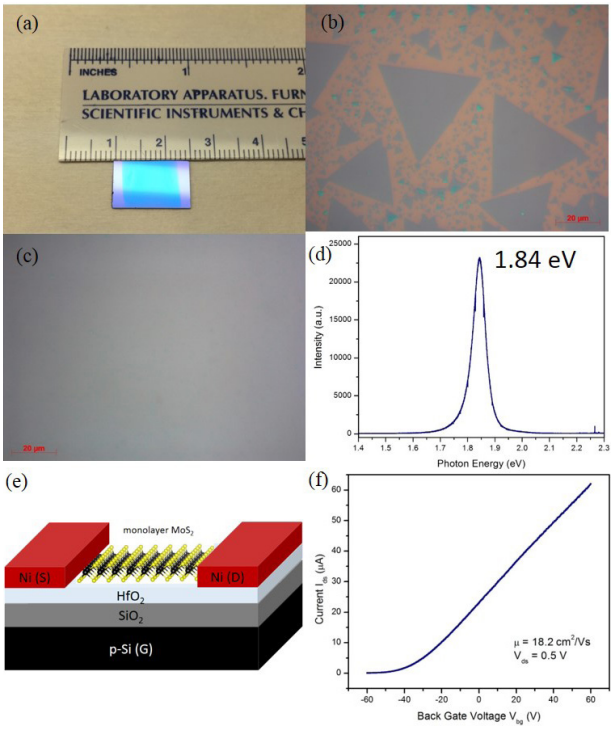

▲ Figure 1: (a) Photo of centimeter-scale monolayer MoS_2 grown on SiO_2/Si wafer. (b) Optical images of CVD-grown triangular domains and (c) completely continuous film of MoS_2. (d) Room temperature PL of MoS_2 films. (e) Schematic of back-gated MoS_2 FET using HfO_2/SiO_2 hybrid gate dielectric and Ni electrodes. (f) Transport properties of single-layer MoS_2 field-effect transmitters (FETs).

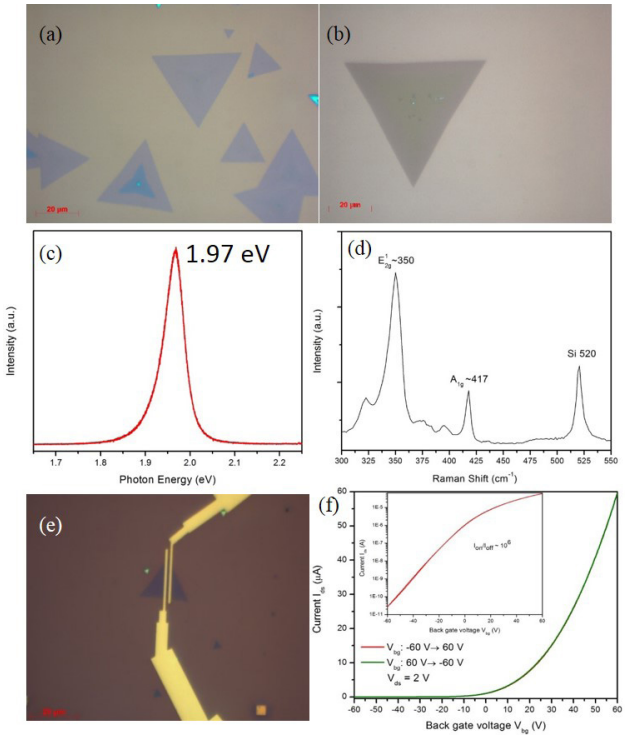

▲ Figure 2: (a) Optical images of as-grown monolayer WS_2 grains. (b) Triangular domain of WS_2 with ~ 65-μm side length. (c) Typical PL and (d) Raman spectra of as-grown WS_2 monolayers. (e) Optical micrograph of typical Ni/WS_2/SiO_2/Si FET. (f) Transfer characteristics of back-gated WS_2 transistor with Ni contacts. (scale bars: 20 μm).

High Speed Roll-to-Roll Production of Atomically Thin (2D) Materials Using a Split Zone CVD Reactor

P. R. Kidambi, D. Mariappan, A. Vyatskikh, M. Feldmann, A. J. Hart
Sponsorship: MIT Energy Initiative, U. S. Department of Energy

Large-area applications of 2D materials such as membranes and barrier films require a means of cost-effective roll-to-roll manufacturing. We have designed and assembled a split zone CVD reactor for roll-to-roll synthesis of 2D materials by chemical vapor deposition (CVD). The reactor configuration consists of an annealing and growth zone separated by a narrow slit through which the catalytic flexible metallic substrate (foil) passes from one end of the reactor to the other. The design of this system was guided by flow simulations. Using the system constructed in our laboratory, we demonstrate synthesis of uniform, high quality graphene at speeds up to 500 mm/min, specifically for membrane and barrier applications. A detailed investigation into the process parameters that influence the growth of graphene on a moving substrate allows us to identify process optimization techniques for roll-to-roll synthesis and subsequent processing for manufacturing of films with tailored nanoscale porosity. We reflect on the scalability of this process and general principles for roll-to-roll CVD of other 2D materials.

▲ Figure 1: Split zone CVD reactor for roll to roll production of 2D materials.

FURTHER READINGS

- P. R. Kidambi, D. D. Mariappan, A. Vyatskikh, M. Feldmann, A. J. Hart, (Manuscript in preparation)
- E. S. Polsen, D. S. McNerny, B. Viswanath, S. W. Pattinson, A. J. Hart, "High speed roll to roll manufacturing of graphene using a concentric tube CVD reactor," *Scientific Reports*, vol. 5, 10257, 2015.
- T. Kobayashi, M. Bando, N. Kimura, K. Shimisu, K. Kadono, N. Umezu, K. Miyahara, S. Hayazaki, et al., "Production of a 100-m-long High-Quality Graphene Transparent Conductive Film by Roll-to-Roll CVD and Transfer Process," *Applied Physics Lett.*, vol. 102, no. 2, 023112, 2013.

Ultrathin High-Resolution Flexographic Printing Using Nanoporous Stamps

S. Kim, H. Sojoudi, H. Zhao, D. Mariappan, G. H. McKinley, K. K. Gleason, A. J. Hart
Sponsorship: MIT Department of Mechanical Engineering, NSF, AFOSR

Since its invention in ancient times, relief printing, commonly called flexography, has been used to mass-produce artifacts ranging from decorative graphics to printed media. At present, higher resolution flexography is essential to the manufacturing of low-cost, large-area printed electronics. However, due to contact-mediated liquid instabilities and spreading, the resolution of flexographic printing using elastomeric stamps is limited to 50-100 μm. Here, we introduce engineered nanoporous microstructures as a next-generation stamp material, comprising polymer-coated aligned carbon nanotubes (CNTs). We design and engineer the highly porous CNT microstructures to be wetted by colloidal inks and to transfer a thin layer to a target substrate upon brief mechanical contact. We demonstrate printing of diverse micron-scale patterns of a variety of functional nanoparticle inks, including Ag, ZnO, WO_3, and CdSe/ZnS, onto both rigid and compliant substrates. The printed patterns have highly uniform nanoscale thickness (5-50 nm) and match the stamp features with high fidelity (edge roughness ~0.2 μm). We derive conditions for uniform printing based on nanoscale contact mechanics, characterize high-conductivity printed Ag lines and transparent conductors after thermal annealing, and achieve continuous printing at a speed of 0.2 m/s. The latter represents a combination of resolution and throughput that far surpasses industrial printing technologies.

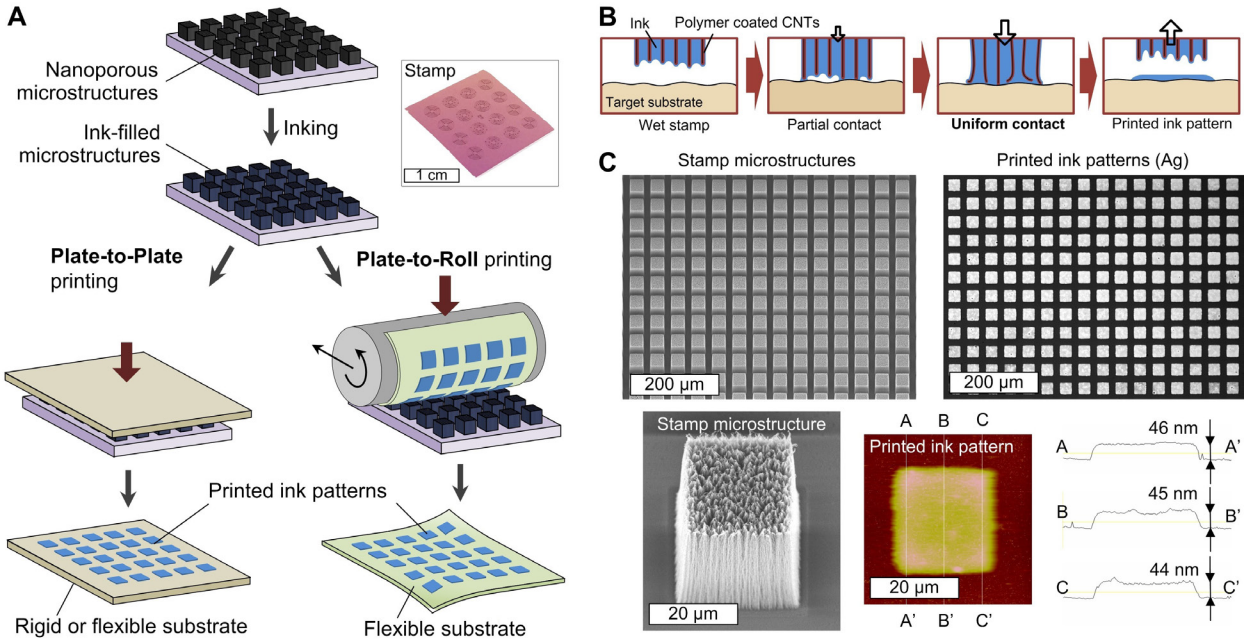

▲ Figure 1: Direct printing of ultrathin colloidal ink patterns using microstructured nanoporous stamps. Schematics of the printing procedure (a) and the uniform transfer of ink (b) from the nanoporous stamp to the target substrate surface via conformal contact, (c) scanning electrode microscopy image of stamp features comprising an array of squares (side length, 25 μm), along with corresponding optical and atomic force microscopy images of the resulting printed Ag ink (particle size, <10 nm; 50-60 weight % in tetradecane) patterns.

FURTHER READING

- P. F. Moonen, I. Yakimets, and J. Huskens, "Fabrication of Transistors on Flexible Substrates: from Mass-Printing to High-Resolution Alternative Lithography Strategies," *Advanced Materials*, vol. 24, 5526-5541, 2012.
- S. Kim, H. Sojoudi, H. Zhao, D. Mariappan, G. H. McKinley, K. K. Gleason, and A. J. Hart, "Ultrathin High-Resolution Flexographic Printing using Nanoporous Stamps," *Science Advances*, vol. 2, e1601660, 2016.

Aligned CNT-Based Microstructures and Nanoengineered Composite Macrostructures

B. L. Wardle, E. Cohen, H. Cornwell, N. Fritz, Y. Gao, R. Kopp, J. Lee, R. Li, D. Lidston, X. Ni, I. Stein
Sponsorship: MIT NECST Consortium, NSF, AFOSR, AFRL, ONR, ISN, NASA NSTRT, NDSEG, NSF Fellowships

Materials comprising carbon nanotubes (CNTs), such as hierarchical nanoengineered advanced composites for aerospace applications, are promising new materials thanks to their mechanical and multifunctional properties. We have undertaken a significant experimentally based program to understand both microstructures of aligned-CNT nanocomposites and hierarchical nanoengineered advanced composites macrostructures hybridized with aligned CNTs.

Aligned nanocomposites are fabricated by mechanical densification and polymer wetting of aligned CNT forests. Here the polymer is typically an unmodified aerospace-grade epoxy. CNT forests are grown to mm-heights on 1-cm² Si substrates using a modified chemical vapor deposition process. Following growth, the forests are released from the substrate and can be handled and infiltrated. The volume fraction of the as-grown CNT forests is about 1%; however, the distance between the CNTs (and thus the volume fraction of the forest) can be varied by applying a compressive force along the two axes of the plane of the forest to give volume fractions of CNTs exceeding 20% (see Figure 1a). Variable-volume fraction-aligned CNT nanocomposites were characterized using optical, scanning electron (SEM), transmission electron (TEM) microscopy, 3-D TEM, and X-ray computed tomography (CT) to analyze dispersion and alignment of CNTs as well as overall morphology. Extensive mechanical property testing and modeling are underway, including 3-D constitutive relations and fracture toughness.

Nanoengineered hierarchical composites hybridized with aligned CNTs are prepared by placing long (>20 μm) aligned CNTs at the interface of advanced composite plies as reinforcement in the through-thickness axis of the laminate (see Figure 2). Three fabrication routes were developed: transplantation of CNT forests onto pre-impregnated plies ("nanostitching"), placement of detached CNT forests between two fabrics followed by subsequent infusion of matrix, and *in-situ* growth of aligned CNTs onto the surface of ceramic fibers followed by infusion or hand-layup. Aligned CNTs are observed at the composite ply interfaces and give rise to significant improvement in interlaminar strength, toughness, and electrical properties. Extensions of the CNT-based architectures to ceramic-matrix nanocomposites and towards multifunctional capabilities are being developed, including structural health monitoring and deicing.

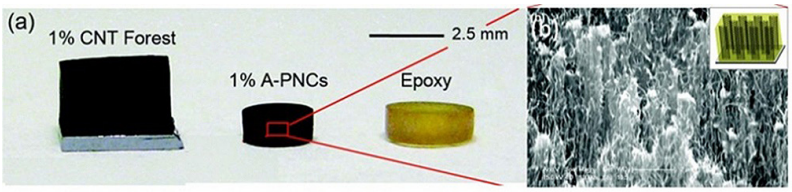

◀ Figure 1. Controlled-morphology polymer nanocomposites: (a) Image of 1% aligned-CNT forest, 1% A-PNCs and pure epoxy samples, (b) SEM image of 1% A-PNCs with an inset schematic of the CNT alignment direction.

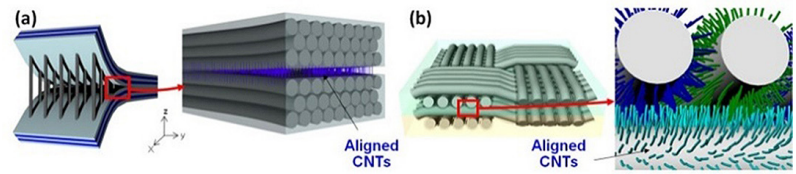

◀ Figure 2: Aligned-CNT nano-engineered composite macro-scale architectures, (a) nanostitching and (b) fuzzy fiber.

FURTHER READING

- L. Gorbatikh, B. L. Wardle, and S. V. Lomov, "Hierarchical Lightweight Materials for Structural Applications," *MRS Bulletin*, vol. 41, no. 9, 672-677, Sep. 2016.
- B. L. Wardle, D. S. Saito, E. J. Garcia, A. J. Hart, and R. Guzman de Villoria, "Fabrication and Characterization of Ultra-High Volume Fraction Aligned Carbon-Nanotube-Polymer Composites," *Advanced Materials*, vol. 20, 2707-2714, 2008.
- B. Natarajan, N. Lachman, T. Lam, D. Jacobs, B. L. Wardle, et al., "The Evolution of Carbon Nanotube Network Structure in Unidirectional Nanocomposites Resolved by Quantitative Electron Tomography," *ACS Nano*, vol. 9, no. 6, 6050-6058, 2015.

Liquid Imbibition in Ceramic-Coated Carbon Nanotube Films

H. Zhao, C. Jacob, H. A. Stone, A. J. Hart
Sponsorship: AFOSR, MITEI

Understanding of the liquid imbibition dynamics in nanoporous materials is important to advances in chemical separations, phase change heat transfer, electrochemical energy storage, and diagnostic assays. We study the liquid imbibition behavior on films of ceramic-coated vertically aligned carbon nanotubes (CNTs). The nanoscale porosity of the films is tuned by conformal ceramic coating via atomic layer deposition (ALD) as shown in Figure 1, enabling stable liquid imbibition and precise measurement of the imbibition dynamics without capillary densification of the CNTs. We show that the imbibition rate decreases as the ceramic coating thickness increases, which effectively changes the CNT-CNT spacing and therefore decreases the permeability. We derive a Darcy's law-based model that incorporates an expression for the permeability of nanoscale post arrays and show that the model fits the experimental results with high accuracy (Figure 2). The tailorable porosity, along with controllable surface wettability and mechanical stability of coated CNTs, suggests their suitability for application-guided engineering and for further investigation of imbibition behavior at finer length scales.

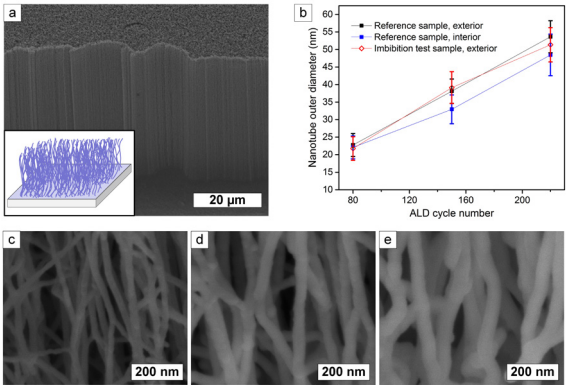

▲ Figure 1: (a) Scanning electron microscopic (SEM) image of an Al_2O_3-coated CNT forest. (b) Outer diameters of Al_2O_3-CNTs as a function of the ALD cycle number. (c-e) SEM images of CNT forests coated with 80, 150, and 220 ALD cycles of Al_2O_3.

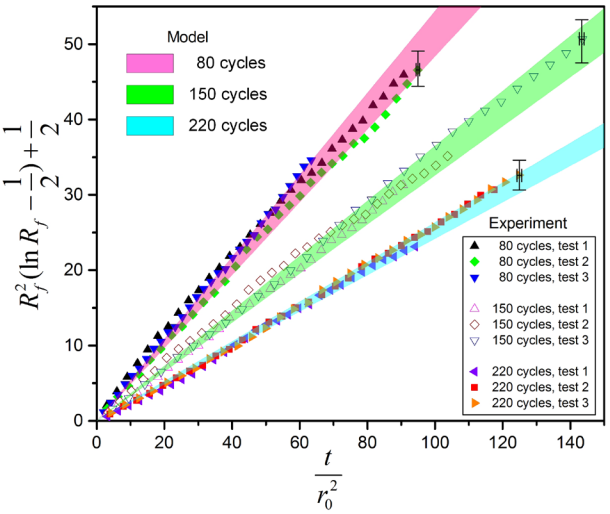

▲ Figure 2: Comparison of model and experiments of liquid imbibition on a 57-μm-tall Al_2O_3-CNT forest, with fitted pitch value p = 78 nm.

FURTHER READING

- H. Zhao, C. Jacob, H. A. Stone, and A. J. Hart, "Liquid Imbibition in Ceramic-Coated Carbon Nanotube Films," *Langmuir*, vol. 32, 12686-12692, 2016.
- A. Brieland-Shoultz, S. Tawfick, S. J. Park, M. Bedewy, M. R. Maschmann, J. W. Baur, and A. J. Hart, "Scaling the Stiffness, Strength, and Toughness of Ceramic-Coated Nanotube Foams into the Structural Regime," *Advanced Functional Materials*, vol. 24, 5728-5735, 2014.

Homogeneous Atomic Fermi Gases

B. Mukherjee, Z. Yan, P. B. Patel, Z. Hadzibabic, T. Yefsah, J. Struck, M. W. Zwierlein
Sponsorship: NSF, ARO, AFOSR, Packard Foundation

We report on the creation of homogeneous Fermi gases of ultracold atoms in a uniform potential. In the momentum distribution of a spin-polarized gas, we observe the emergence of the Fermi surface and the saturated occupation of one particle per momentum state: the striking consequence of Pauli blocking in momentum space for a degenerate gas. Cooling a spin-balanced Fermi gas at unitarity, we create homogeneous superfluids and observe spatially uniform pair condensates. For thermodynamic measurements, we introduce a hybrid potential that is harmonic in one dimension and uniform in the other two. The spatially resolved compressibility reveals the superfluid transition in a spin-balanced Fermi gas, saturation in a fully polarized Fermi gas, and strong attraction in the polaronic regime of a partially polarized Fermi gas.

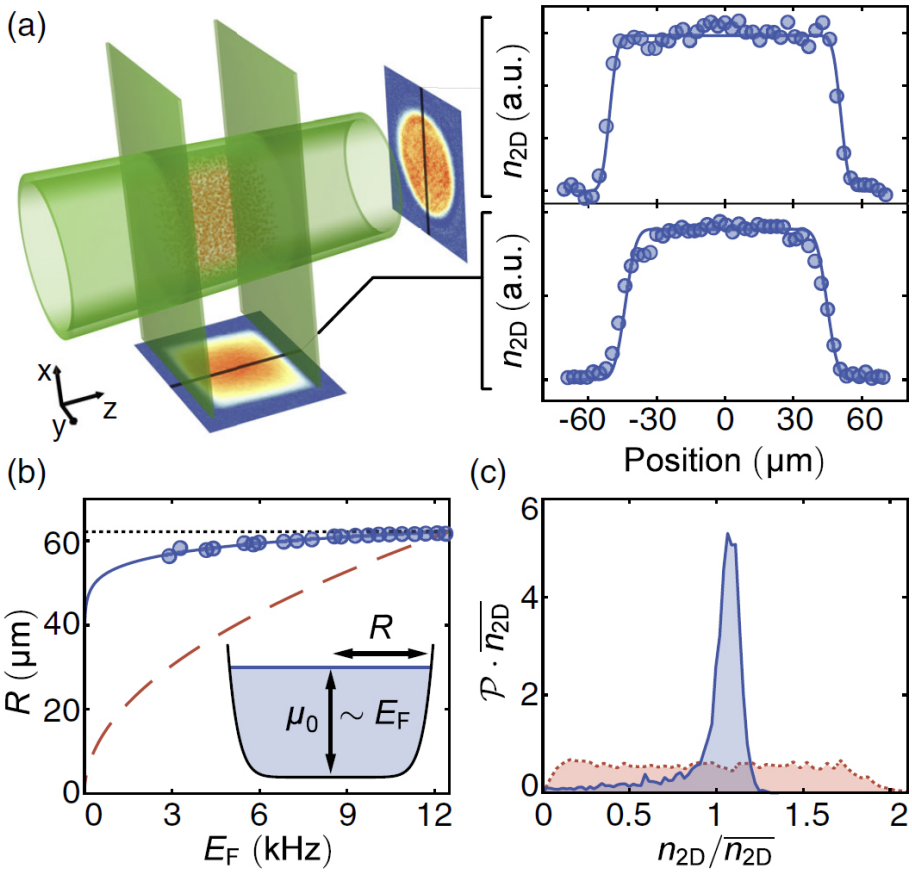

▲ Figure 1: Homogeneous Fermi gas. (a) Schematic of box trap and cuts through column-integrated density profiles along axial and radial directions. (b) Radius of cloud as function of Fermi energy. Dotted black and dashed red lines correspond to perfect box potential and harmonic potential, respectively, and are scaled to converge at highest E_F. Blue solid line corresponds to power law potential $V(r) \sim r^{16}$. (c) Measured radial probability density $P(n_{2D})$ for column integrated density n_{2D}, averaging about 20 in-trap images. Blue solid and red dashed lines correspond to uniform and gaussian traps, respectively.

FURTHER READING

- B. Mukherjee, Z. Yan, P. B. Patel, Z. Hadzibabic, T. Yefsah, J. Struck, and M. W. Zwierlein, "Homogeneous Atomic Fermi Gases," *Phys. Rev. Lett.* 118, 123401, 2017.